Spatiotemporal Electrochemical Sensing in a Smart Contact Lens

Spatiotemporal Electrochemical Sensing in a Smart Contact Lens

Matthew Donora[a,], Andrés Vásquez Quintero[b], Herbert De Smet[b] and Ian Underwood[a]*

[a] School of Engineering, University of Edinburgh, UK

[b] Centre for Microsystems Technology, Ghent University, Belgium

Keywords: smart contact lenses, electrochemical sensing, non-invasive devices, biosensors, microelectrode arrays

Abstract

An electrochemical smart contact lens (ESCL) capable of real-speed spatiotemporal electrochemical sensing across the surface of the eye is demonstrated. Four microelectrode arrays, each comprising 33 gold microdiscs of 30 μm diameter, and a distributed common gold counter electrode, are integrated into a soft smart contact lens platform based on polyimide and thermoplastic polyurethane. Using a novel fast-switching chronoamperometric method, an electrochemical 'video' of concentration variation in a model eye under flow conditions is produced, in which the introduction, progress, mixing and drainage of fluid of varying concentration can be observed. The device builds on previous work towards a platform suitable for clinical use and has proven to be robust under expected use conditions, with sensing performance remaining unchanged after thermoforming and repeated mechanical deformation. This work represents a significant step forward in ESCL design, and constitutes significant progress towards a technology with real clinical utility.

1 Introduction

Non-invasive medical devices such as smart contact lenses (SCLs) are set to revolutionise the way we approach medicine and healthcare. The ability to unobtrusively monitor health parameters while a patient goes about their day has a number of significant benefits, such as providing clinicians with more (and more useful) diagnostic information, saving time and hospital resources, and improving

patients' quality of life. SCLs are a promising class of non-invasive medical device. An FDA-approved SCL is already used to monitor intra-ocular pressure for glaucoma treatment.[1] There is high potential for new functionalities to be integrated into SCLs, and work towards active vision correction,[2,3] drug delivery,[4] display technology[5,6] and chemical sensing[6–8] is under way. Electrochemical smart contact lenses (ESCLs) may be used to monitor chemical markers found in the tear film, and are therefore of particular interest to the field of medical diagnostics [9,10]. Many biomarkers found in blood are well represented in the tear film,[11] including glucose,[12] lactate,[13] hormones such as cortisol, serotonin and dopamine,[14] and many others. An ESCL may therefore be an excellent candidate for non-invasive monitoring of various biomarkers traditionally measured in blood. Chemical measurement in the tear film is not only far less invasive than a blood test, but can be performed continuously and unobtrusively while a patient carries out normal day-to-day tasks. This allows us to see time-series trends in the biomarkers, which provides far more diagnostic information than intermittent 'snapshot' measurements. Continuous, unobtrusive monitoring is of great clinical importance for (e.g.) hormones such as cortisol, serotonin and dopamine,[14,15] and is currently almost impossible to perform outside of a hospital setting. In diagnosing and investigating conditions where psychological elements are currently better understood than physiological, such as depression,[16,17] chronic stress,[15,18] addiction,[19] PTSD[20] and more, unobtrusive continuous sensing of hormonal trends could allow unprecedented insight into the physiological processes underlying these disorders.

However, despite significant effort in moving towards clinical applications, ESCL prototypes have not yet progressed past the research stage. Issues with materials (such as polyethylene terephthalate (PET),[7] which exhibits buckling behaviour after moulding)[21] have largely been addressed in other SCL research, with (e.g.) a state-of-the-art SCL platform utilising polyimide and thermoplastic polyurethane (TPU) developed for active vision correction.[22] Polyimide is a biocompatible polymer,[23,24] and, due to its high glass transition temperature of 360 °C[25] and liquid-state processing, can form layers of a few microns in thickness which are subsequently

compatible with most cleanroom processes.[26] Due to these favourable properties and its flexibility and strength, polyimide has been increasingly commonly used in research towards flexible electronics intended for biomedical use.[27–30] TPU is also a biocompatible polymer,[31] and can be thermoformed at relatively low temperatures (< 150 °C) to create moulded hemispherical devices which exhibit no buckling behaviour.[22] Adapting this platform to ESCL designs will improve the mechanical and physical properties of the device significantly. Other materials (such as PDMS [32,33]) have been demonstrated for SCL design at the prototype stage, though a robust microfabrication pathway fulfilling all the design criteria of an ESCL has not been developed using alternative materials at this stage. However, this is not the only issue facing ESCL design.

Reported prototypes have so far focussed primarily on glucose monitoring for diabetes management,[6,7] with one lens also investigating lactate,[8] but concerns about the measurement fidelity and time delay from blood glucose to tear glucose have presented significant problems in the route to clinical use.[12,34,35] Generally, these prototypes have all made the gross oversimplification of treating the tear film akin to a bulk fluid, but the reality is that the tear film is a complex fluid environment. Tear fluid enters the eye from the lachrymal ducts, progresses across the surface of the cornea under influence of fluid effects, blinking and gravity, and drains into the nasal-lachrymal duct via the lachrymal puncta.[36,37] In addition, evaporation, atmospheric humidity, ‘reflex’ or ‘emotional’ tears, and even exposure to rain can affect concentration levels in the eye in ways that are uncorrelated to the base variation of concentration in blood. It is therefore insufficient to measure concentration in some part of the tear film (most likely the indeterminately mixed region of the lachrymal lake), and expect enough fidelity in the measurement to reliably reconstruct concentration levels in blood. We must seek more information about the introduction, mixing and drainage of the lachrymal fluid if we are to achieve a desired level of confidence in the electrochemical measurements we make there, and therefore reach useful diagnostic conclusions. In

short, we must track the spatiotemporal concentration of biomarkers across the surface of the cornea.

Previous ESCL designs have generally used macroelectrodes;[7,8] however, micro- and nanoelectrodes exhibit enhanced sensing properties when compared to macroelectrodes, such as increased sensitivity, improved mass transport and faster response times,[38,39] attributes which are of particular utility when sensing in the tear film (i.e. a dilute, low-volume media) and when performing high-speed measurements (such as those used in our fast-switching chronoamperometric method).[40] Using microelectrodes also greatly improves the form factor of the ESCL, and reduces power requirements, since they draw less current than macroelectrodes. Because of their smaller size, many microelectrodes may be placed on one ESCL, for spatiotemporal sensing, multimodal analysis (i.e. functionalising for various different biomarkers on the same device), or both. To achieve a higher signal-to-noise ratio without sacrificing the enhanced sensing properties of single microelectrodes, connected arrays of microelectrodes may be used.

In this work we present a next-generation ESCL with four individually addressable microelectrode arrays distributed in the four quadrants of the lens, and demonstrate our fast-switching chronoamperometric technique, which allows real-speed spatiotemporal sensing of concentration variation across the surface of the eye. We demonstrate this functionality in an eye model, with fluid flow mimicking that found in the eye, and observe real-speed spatiotemporal electrochemical measurement of this concentration flow. This device represents a step forward in how we approach electrochemical measurement in smart contact lenses, and paves the way for a new generation of devices on the path to clinical use.

2 Materials and Methods

Device Fabrication

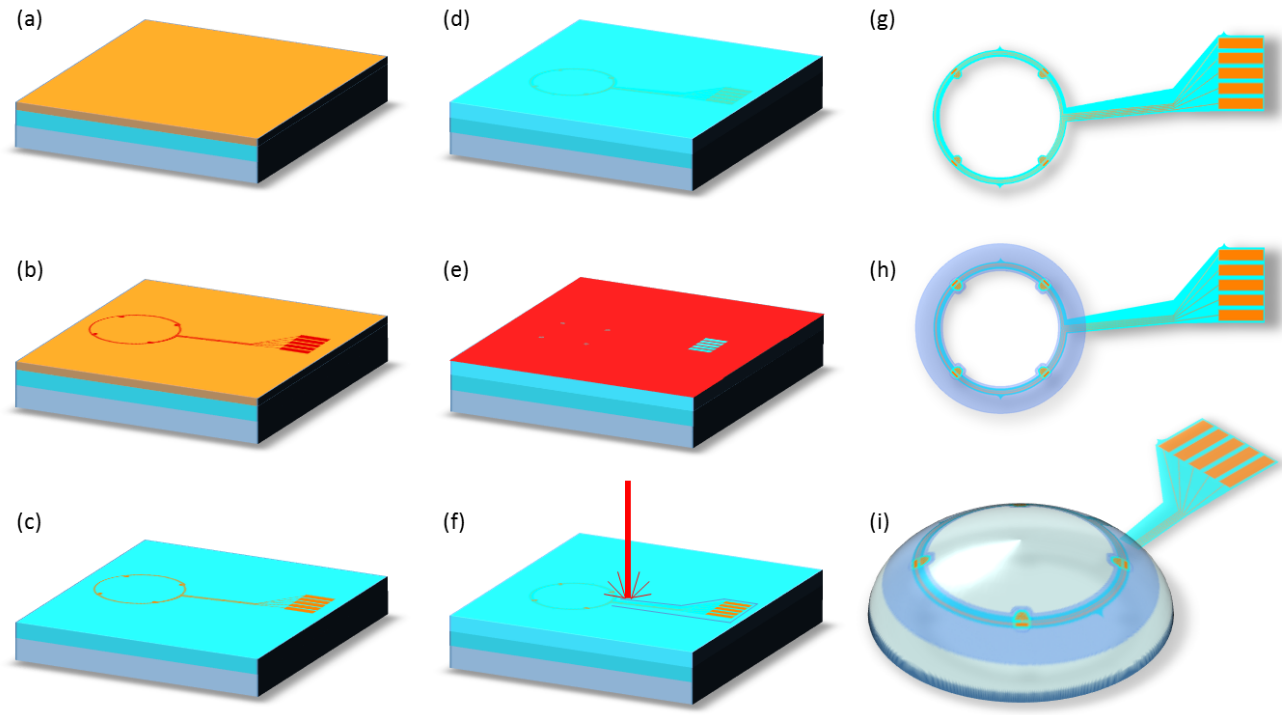

Figure 1. Diagrammatic representation of fabrication steps: (a) Polyimide and TiW/Au layers on a glass wafer; (b) S1818 resist patterned to define metal layers; (c) metal layers defined by wet etching and stripping of photoresist; (d) polyimide layer spin-coated over metal layers; (e) thick photoresist (AZ4562) patterned to define contact pads and electrode sites; (f) after reactive ion etch and stripping of photoresist, a picosecond laser is used to cut out the device; (g) device released from glass wafer; (h) pre-patterned thermoplastic polyurethane bonded on either side of the device, and device cut to shape using a picosecond laser; (i) device thermoformed to a spherical cap shape and added to hydrogel contact lens.

The device fabrication process is illustrated in **Figure 1** and described below. A layer of polyimide (5.5 μm) was spin-coated onto a cleaned glass wafer, dried on a hot plate and cured in a nitrogen oven. Metal layers of TiW (50 nm, adhesion layer) and Au (100 nm) were deposited by sputtering. These metal layers were patterned with photolithography (S1818 photoresist) and wet etching. A second layer of polyimide was added as described above. Thick photoresist (AZ4562, target thickness 10 μm) was used as a hard mask to define contact pads and electrode sites, and reactive ion etching (45 min, 22 sccm O_2, 5 sccm N_2, 350 mTorr, 75 W; or using previously described

parameters in)[40] was used to etch the top layer of polyimide through to the gold layer. The photoresist was stripped and the devices cut out using a picosecond laser (355 nm, 12 ps, 50 kHz, 320 mW). The devices were then released from the glass wafer using thermal release tape. Thermoplastic polyurethane was pre-patterned with the picosecond laser (355 nm, 12 ps, 50 kHz, 400 mW, 10 passes at 40 mm s^{-1}), creating vias at the electrode sites and contact pads. These pre-patterned sheets were bonded to either side of the devices with a custom two-step method using a wafer bonder. The encapsulated devices were once again cut out using the picosecond laser (same parameters as previous step) and moulded into a hemispherical cap shape with thermoforming.

Electrochemistry

Ferrocenemethanol (Aldrich, 97% purity) was prepared in various concentrations in 0.1 M potassium chloride (Aldrich, 99% purity) with deionised water. All devices were electrochemically cleaned in H_2SO_4 with 5 cycles of cyclic voltammetry (0 V – 1.6 V – 0 V). Electrochemical experiments were carried out in a Faraday cage using an Autolab PGSTAT128N potentiostat, using the on-device gold counter electrode and an external Ag/AgCl counter electrode (BASi, USA). Control and data acquisition was performed using Nova 2.0.1.

During spatiotemporal sensing a 74HC4051 8-channel analog multiplexer, driven by a microcontroller (Arduino Nano)[41], was used to rapidly switch in sequence through the eight working electrodes. Data processing was carried out using algorithms written in the python programming language.

Eye Model

An eye model (see Appendix D) was constructed using Newplast (modelling clay), silicone tubing and a polymer (polyoxymethylene) sphere. While a real eyeball has an overall radius of around 12 mm, contact lenses usually have radius of curvature closer to 9 mm to account for the shape of the cornea; thus, a sphere radius of 9 mm was chosen. Fluid was added via the fluid input tube

(placement chosen to mimic the location of the lachrymal ducts), and drained through or over the fluid output tube (placement chosen to mimic the location of the lachrymal puncta). Fluid contact at the electrode surfaces, and between the three active electrodes (counter, reference, and the active working electrode) is required for electrochemical sensing; without this, the characteristic chronoamperometric sub-signal would not be observed. To ensure fluid contact during the eye model experiment, the surface of the model eye was irrigated, followed by placement of the pre-wetted SCL, followed by another surface irrigation, both topically and through the fluid input tube.

3 Results and Discussion

3.1 Device Design

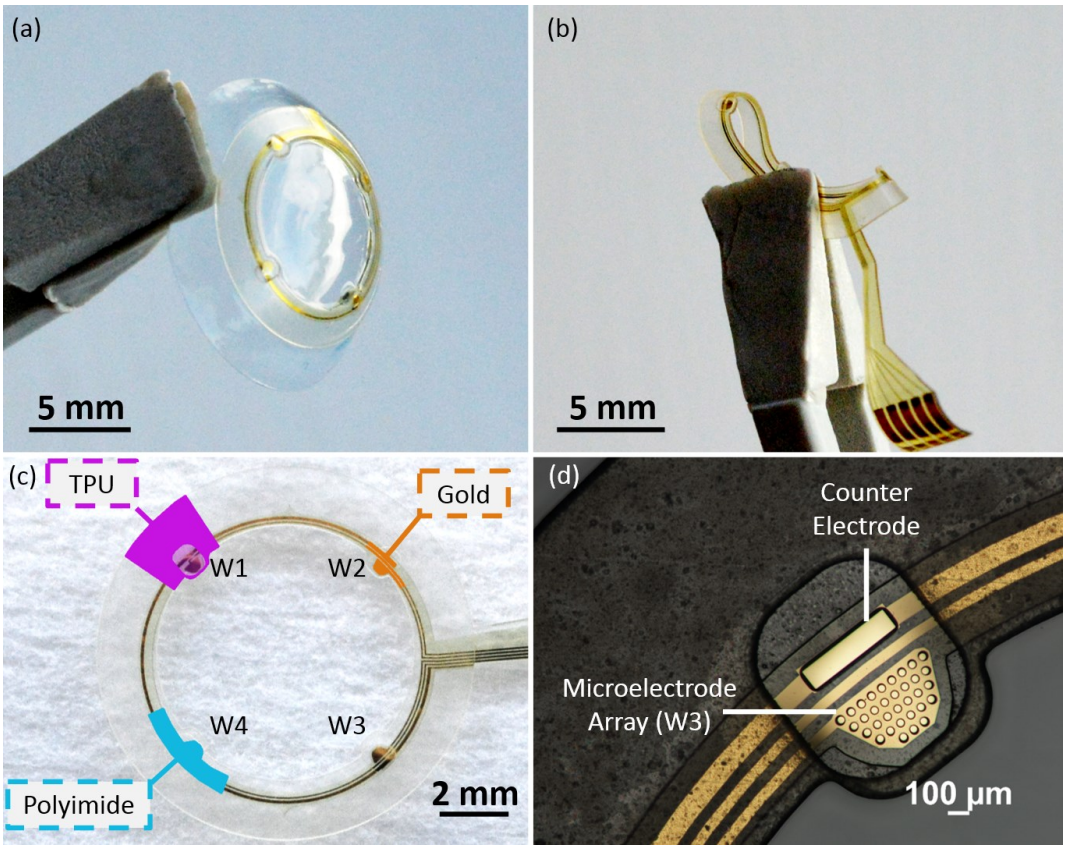

Figure 2. Images of the ESCL device. (a) Photograph of the ESCL device illustrating placement on a contact lens; (b) photograph of the ESCL undergoing mechanical deformation using tweezers. (c) Photograph of an unmoulded ESCL, illustrating material regions. Working electrodes 1-4 are indicated by W1-4; (d) photo micrograph of working electrode 3 (W3).

This ESCL (**Figure 2** a) consists of a core device – comprising a layer of gold (100 nm in thickness, with a 50 nm titanium-tungsten adhesion layer), sandwiched between two layers of polyimide, each 5.5 μm in thickness – which is encapsulated in two layers of TPU, and moulded to a spherical cap shape (radius of curvature 9 mm). The device is flexible and robust to folding (Figure 2 b), returning to its original shape after repeated mechanical deformation.

Previous work has shown that serpentine connections may reduce buckling behaviour in the substrate after thermoforming;[22,42] however, since these were only necessary in the radial direction, we restricted our design area to a narrow ring in the circumferential direction of the lens. Previous work also highlighted the necessity of reducing parasitic capacitance, inductance and resistance in an ESCL device;[40] using non-meandering connections to the electrode sites, we were able to significantly reduce these effects. Straight connections were also more spatially efficient, and therefore reduced the physical footprint of the device – this reduction is likely to improve comfort during normal use.

In practice, oxygen permeability is a key factor in contact lens comfort and safety. Modern contact lens materials are highly oxygen permeable,[43] and, unlike many reported ESCL prototypes, the ring-shaped design of this ESCL leaves the majority of the lens area free from non-oxygen-permeable materials, allowing sufficient oxygen transfer to the eye for safe extended use.

The ESCL consists of a set of four individually addressable microelectrode arrays, with one placed in each quadrant of the device (Figure 2 c). Each is situated next to one of four counter electrodes (Figure 2 d), which share a single electrical connection. Each microelectrode array comprises 33 microdisc electrodes of 30 μm diameter, spaced at 30 μm in the planar orthogonal directions, in an offset grid of a custom shape (Figure 2 d). The shape of the microelectrode arrays was chosen to optimise spatial efficiency and reduce deviation from the design area.

The close proximity of the microdisc electrodes within each array is such that, at longer time scales of continuous current flow, the individual diffusion fields overlap and reduce the sensing

performance of the system (i.e. the sensor would subsequently perform akin to a larger electrode comprising the entire area of the array). An estimate of this time scale can be made using Fick's law, with overlap time t_{ov} occurring at approximately

$$t_{ov} = \frac{{L_{diff}}^2}{2D}, \quad (1)$$

Where L_{diff} is the characteristic size of the diffusion field and D is the diffusion coefficient of the redox species (here we use ferrocenemethanol, with a value of $D = 5\times10^{-10}$ m^2 s^{-1}.[44] For a physiological comparison, cortisol has a diffusion coefficient of $D_{cortisol} \approx 2.9\times10^{-10}$ m^2 s^{-1}).[45] Using $L_{diff} = 15$ μm, we find $t_{ov} \approx 225$ ms. Our sensing technique uses fast-switching chronoamperometry which operates for less than 50 ms at a time. Thus, the microdisc spacing is sufficient to achieve microelectrode-like sensing characteristics during intended use.

In this study we used a ZIF connector to interface the device; placement of a thinned silicon chip has been described in previous work,[22,46,47] and this ESCL is intended to function wirelessly, once sensing protocols have been established. Using an antenna to harvest power inductively,[46] power transfer of greater than 100 μW has been demonstrated,[5] and new flexible battery technologies developed for smart contact lenses also lead to stringent power requirements.[48] Thus, a balance was required in designing the microelectrode arrays: increased current reduces the required sensitivity of the potentiostat system, and can lead to a more robust and compact chip design, and increase the signal to noise ratio. However, higher current leads to increased power requirements. Using previous work as a guide,[40] we calculated that the fast-switching chronoamperometry sensing protocol draws an average of approximately 1 μA, including parasitic circuit effects. At 0.4 V, this leads to an estimated power consumption of approx. 13.5 μW with 33 arrayed microdisc electrodes – that is, similar to the power transfer to the active element demonstrated by Pandey *et al.*[5] However, our design for the ESCL device significantly reduced these parasitic effects, and in fast-switching chronoamperometry the microelectrode arrays draw

only approx. 40 nW (Section 3.3). Therefore, this system falls very comfortably within the power requirements of current SCL platforms.

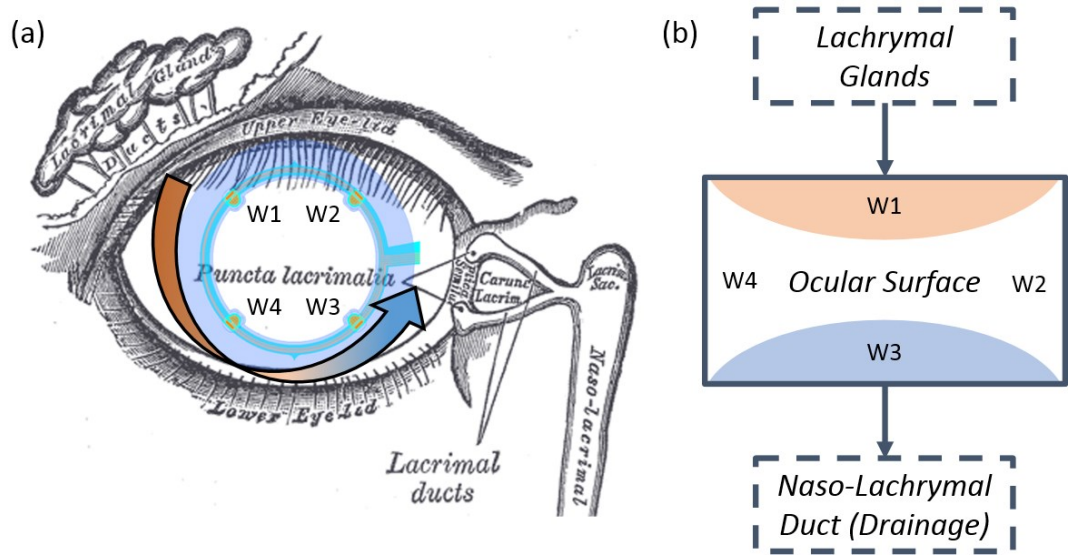

Figure 3. Illustration of fluid flow in the eye. (a) Illustration of the anatomy of the eye, and the placement of the ESCL on the corneal surface. The arrow indicates overall flow of tear film from source to drain. Some parts of this figure reproduced from Gray's Anatomy, Plate 896; (b) schematic illustration of a three-compartment model of lachrymal fluid introduction, progress and drainage.

The placement of the electrodes in each of the four quadrants of the ESCL was chosen to investigate the flow of chemical markers across the cornea, with reference to the position of the tear film source (the lachrymal ducts) and drain (the lachrymal puncta) (**Figure 3** a). With spatially distributed sensing, more information about the introduction, progress and drainage of chemical markers in the lachrymal fluid may be gathered. For example, W1 might measure an increased concentration in new lachrymal fluid as it enters the eye; W4 and W2 provide information on the bulk tear fluid (i.e. within the lachrymal lake); and W3 provides information on the concentration at the point of drainage. Using these data and an appropriate three-compartment model, as shown schematically in Figure 3 b, an estimation can be made of the current concentration level in the lachrymal glands, giving the earliest possible indication of changes of the concentration in the rest

of the body (particularly in blood). Earlier ESCL prototypes have struggled to measure markers (such as glucose) with sufficient fidelity and speed to make useful estimations of current blood glucose levels;[12] using this spatiotemporal method, we may be able to improve measurement fidelity sufficiently to make accurate diagnostic conclusions, and even early-warning health monitoring systems, using an ESCL.

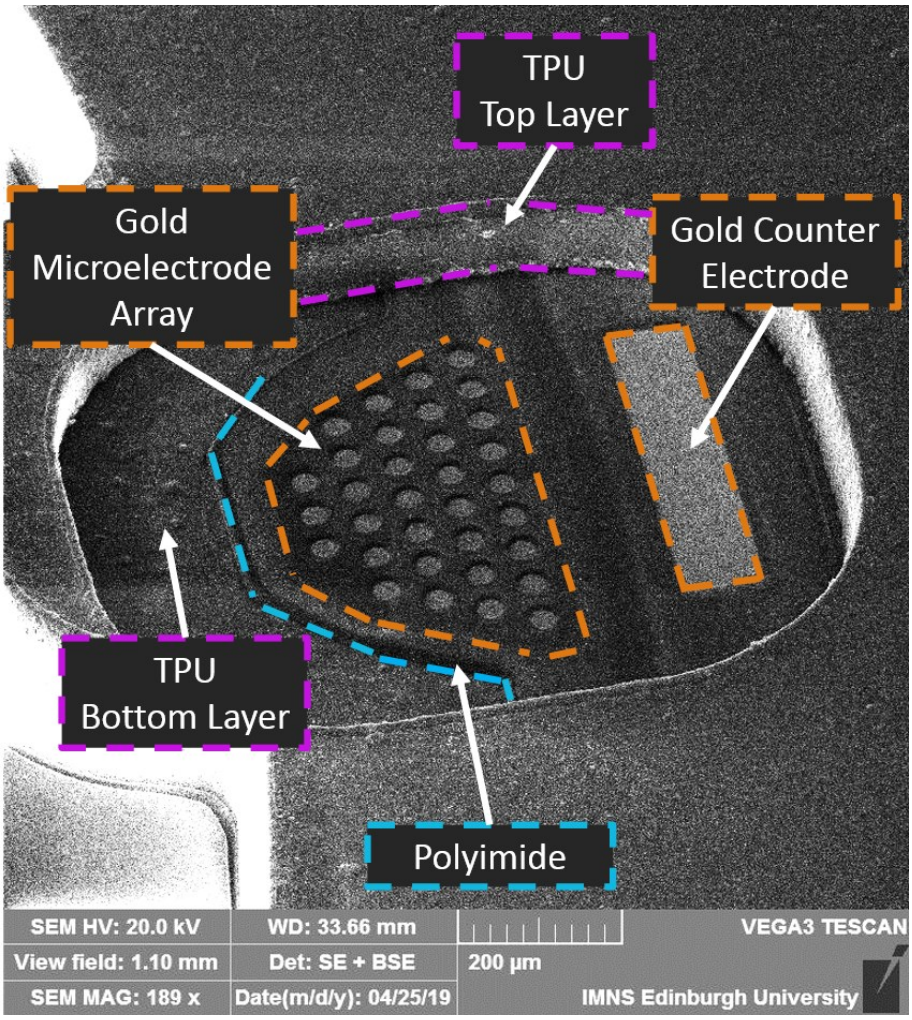

Figure 4. Scanning electron micrograph of a working electrode site.

Previous ESCL designs have not explicitly reported the question of efficient tear film contact with the electrochemical sensors, generally assuming instead a bulk fluid scenario. However, integration of a device such as this into a contact lens likely entails encapsulation in hydrogel or a similar material. In addition, it is currently unclear whether the best position for the sensors is out- or in-facing. The current model of the tear film describes a bi-layer structure, with a thin superficial lipid

layer and an aqueous/mucin gel layer with decreasing mucin content from the corneal surface to the lipid layer,[36] and it is not currently understood exactly how the addition of a contact lens affects this structure. It is possible that different analytes may variously be better represented on either the out- or in-facing side of the lens, depending on their representation in each fluid environment (i.e. aqueous, mucosal or lipid), and therefore two classes of ESCL or a combined lens may be necessary. Corneal irritation must be considered in the in-facing case. In this ESCL, the sensing sites are recessed 100 μm into the TPU surface (**Figure 4**), which is greater than the estimated depth of the tear film (40 μm),[49] and it is not yet known whether this architecture would cause irritation or discomfort if placed in direct contact with the ocular surface. In this study we moulded both in- and out-facing lenses, and observed no difference in performance. The out-facing lenses were estimated to be more suited to the ocular environment, and this architecture is also less likely to cause irritation in the eye. However, in-facing sensors may experience less interference from environmental effects such as rain and humidity. A more in-depth investigation into this question may be useful on the route to clinical use, though it is outside the scope of this particular work.

Partial and full hydrogel encapsulations are both possible. For a partial encapsulation, the active side of the ESCL may be left exposed to allow for tear film contact; for a full encapsulation, analyte diffusion through the hydrogel may be sufficient for electrochemical sensing, or active functionalised hydrogels may be used to avoid the need to rely on diffusion.[50] Direct windows to the sensing sites may be created in the hydrogel, akin to those in the TPU top layer (Figure 4). Alternatively, channels could be etched into the hydrogel to provide flow access to the sensors, perhaps with a passive blink-mediated pumping system to improve fluid transport (similar to musculovenous pumping).[51] However, irritation might occur at the window or channel sites, and biofouling could result in significant flow problems.

Functionalisation of the electrode sites may be performed in bulk, or with more precision using inkjet printing methods. Future ESCL designs could include additional sets of microelectrode arrays

in each quadrant, which may be functionalised differently to measure a number of different analytes in the same lens. Differential or multimodal use may improve diagnoses, measurement fidelity, and cost efficiency of a device. In this design an external reference electrode was used, but on-board reference electrodes have been demonstrated for ESCL designs,[52] and, since they are used in common with each electrode, would not increase design footprint significantly.

3.2 Electrochemical Characterisation

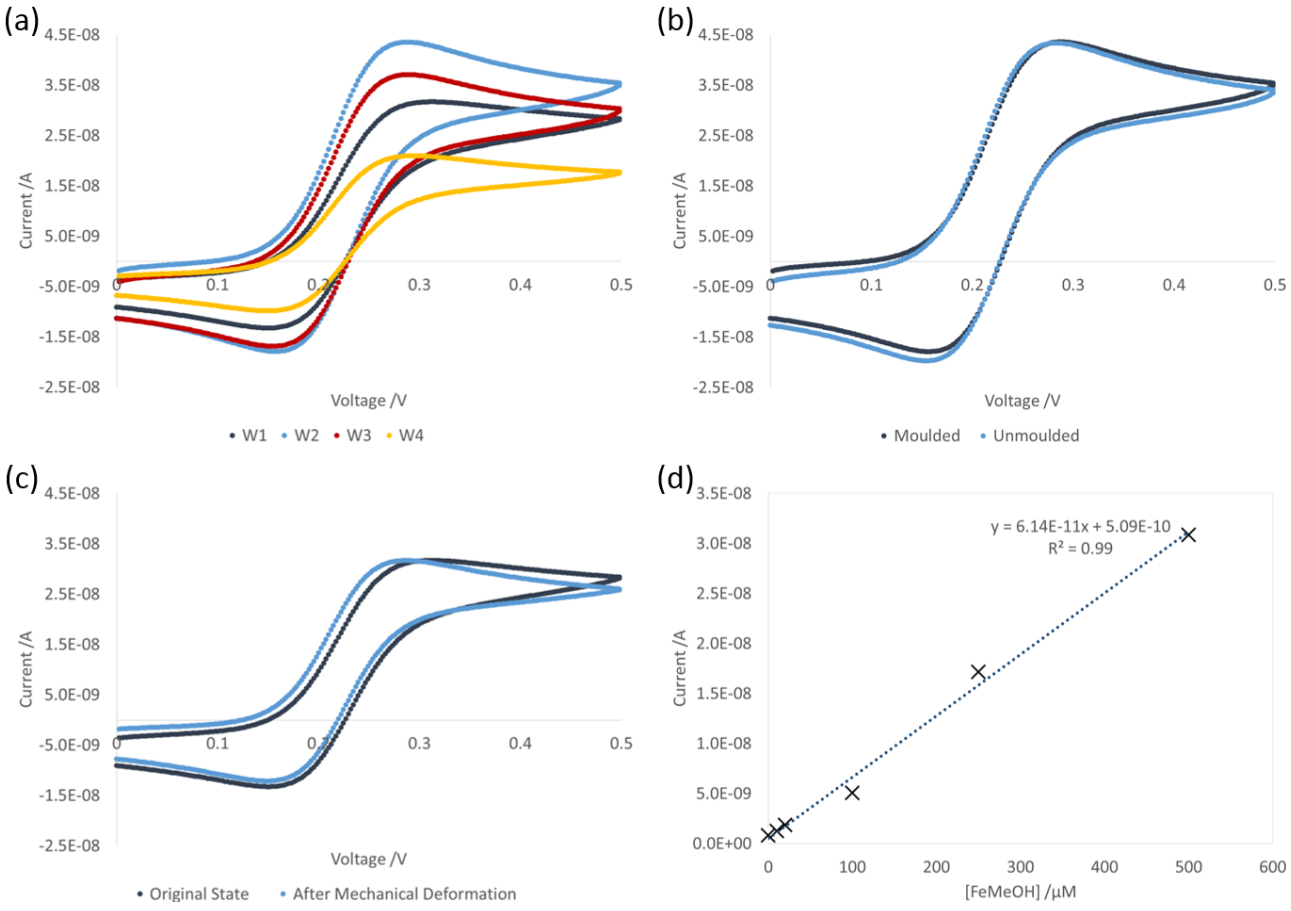

Figure 5. Electrochemical characterisation of the microelectrode arrays. (a) Cyclic voltammograms of each working electrode in a single lens; (b) cyclic voltammograms taken before and after moulding; (c) cyclic voltammograms taken before and after repeated mechanical deformation; (d) current response to a range of concentrations of FeMeOH.

Electrochemical characterisation was carried out using standard cyclic voltammetry (0 V – 0.5 V – 0 V, at 0.1 V s^{-1}), in 0.5 mM ferrocenemethanol (FeMeOH) – a redox reporter which exhibits well-

characterised electrochemical behaviour at bare metal electrodes, and is often used to investigate electrochemical systems. The microelectrodes showed expected sensing characteristics in these experiments; however, it is worth noting that these arrays were designed for high-speed sensing protocols (Section 3.1), and therefore diffusion field overlap may result in reduced sensitivity during these standard tests.

Variation in current response between the different electrode sites was observed (**Figure 5** a). In previous work, the effect of surface roughness was quantified and discussed,[40] and the intra-lens variation here is likely due in part to a non-uniform reactive ion etch profile during fabrication (faster etch speeds were observed at the periphery of the wafers than at the centre), which resulted in higher surface roughness in some electrodes. In addition, misalignment of the TPU windows caused physical fouling of the electrode surfaces during the last laser excision stage in some electrode sites, and to varying degrees between electrode sites, which may also account for the observed variation (see Appendix A). This variation is corrected for during normalisation in the high-speed chronoamperometric sensing protocol.

Sensing performance before and after thermoforming was investigated, and no difference was found between the two states (Figure 5 b). Similarly, sensing performance was unchanged after repeated mechanical deformations (Figure 5 c; ten full folds of the lens, as illustrated in Figure 2 b). The position of the metal layer in the neutral mechanical plane reduces stress during mechanical deformation to a minimum and avoids cracking or damage to the wire tracks.

Comparison of these results to an established theoretical model of microdisc electrodes was carried out using the Saito equation (equation (2)),[53] which calculates limiting current under steady-state conditions:

$$i_L = 4nFDc_0r \quad (2)$$

Where n is the number of electrons transferred in the reaction, F is the Faraday constant, D is the diffusion coefficient of the redox species (FeMeOH), c_0 is the concentration, and r is the radius of the microdisc. We used values of $D = 5\times10^{-10}$ m^2 s^{-1},[44] and $c_0 = 0.5$ mol m^{-3}. In addition, theoretical models suggest that the recession of a microdisc electrode of radius 15 μm into the polyimide by 5.5 μm will result in a reduction in current drawn by 32%;[54] this correction is included our analysis. A mean limiting current from the four electrodes was found to be 3.01×10^{-8} A, which in this model yields a microdisc radius of 13.8 μm (for an array of 33 microdiscs). This is slightly smaller than the true size, a reduction which may result from physical fouling of some of the electrode surfaces by TPU during the last laser excision stage (see Appendix A).

Cyclic voltammetry was also used to investigate linearity of the current response to a range of concentrations of FeMeOH, from 10 to 500 μM, and a 'blank' measurement of KCl (0.1M) (Figure 5 d). As seen in previous work,[40] a linear current response was observed, with $R^2 > 0.99$, indicating a high confidence in the linear fit. Limit of detection (LOD) was calculated following the IUPAC convention:[55]

$$x_L = \bar{x}_{bl} + ks_{bl} \quad (3)$$

where x_L is the smallest current that can be reliably detected, $\bar{x}_{bl}$ and s_{bl} are the mean and standard deviation respectively of the blank (KCl) measurement, and k is a numerical factor (we used $k = 3$ to ensure a confidence level of > 99%). The LOD is obtained by substituting $x = x_L$ into the calibration function (Figure 5 d), yielding the lowest detectable concentration at this confidence level. Despite the close proximity of the microdiscs in the array (Section 3.1), we calculated a LOD of 7.8 μM. This is a twofold improvement on previous results,[40] most likely due to the increased signal (and therefore higher signal-to-noise ratio) of the microelectrode array.

3.3 Spatiotemporal Electrochemical Sensing

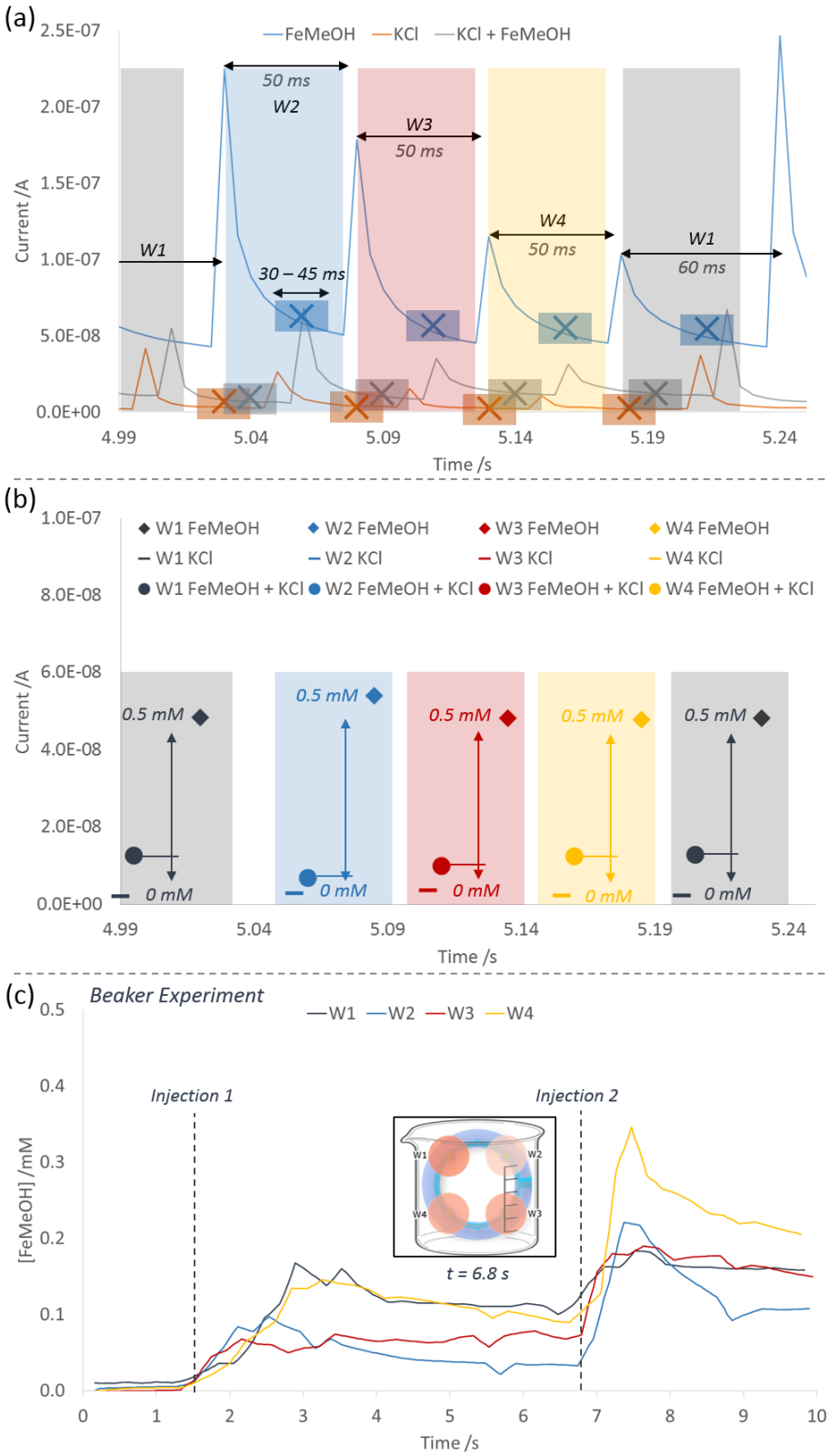

Figure 6. Illustration of the signal processing method. (a) Raw signal from fast-switching chronoamperometry in high concentration ('FeMeOH'), zero concentration ('KCl') and varying

concentration ('KCl + FeMeOH'). Extraction of a single data point from each chronoamperometric sub-measurement is denoted by crosses; (b) calibration procedure using the extracted data points from *(a)*, in which varying concentration measurements are compared with temporally-aligned high and zero measurements; (c) calibrated concentration data for each working electrode during a full 10 s experiment with varying concentration in a beaker. Two injections of FeMeOH into an initial volume of KCl are indicated. Inset: visual representation of the concentration at each working electrode, with concentration values represented by red colour shading (see Video 1).

Spatiotemporal electrochemical sensing was performed using an updated version of our fast-switching chronoamperometric method.[40] An analogue multiplexer driven by a microcontroller (Arduino Nano)[41] was used to address the working electrodes one-by-one in a cyclic sequence. Working electrode 1 (W1) was addressed for 60 ms, while W2-4 were addressed for 50 ms; this variation was used to tag W1 for easier signal separation. The sequence resulted in a frame rate of approximately 19 Hz (i.e. 19 electrodes per second). A potentiostat performed a chronoamperometric measurement (10 s, 0.4 V, 200 Hz sample rate) while the switching cycle repeated (see Appendix B for schematic representation of the circuit). In combination this produced a signal effectively consisting of a repeating four-step sequence of 50 ms (or 60 ms) chronoamperometric measurements (**Figure 6** a). The 30-45 ms period within each measurement was isolated and, taking the arithmetic mean of the data within this period, a single current value was calculated at that time point (Figure 6 a). The time period was chosen to avoid non-Faradaic signal at the beginning of the chronoamperometric measurement and any switching noise at the end. For each experiment, a full (10 s) measurement was performed in 0.1 M KCl (a zero concentration measurement) and 0.5 mM FeMeOH (a high concentration measurement), before spatiotemporally-varying concentration profiles were investigated. Having established the linearity of the current-concentration relationship (for this range) in Section 3.2, these measurements were used to calibrate each electrode at each time point, as shown schematically in (Figure 6 b). Since each electrode was updated every four frames, linear interpolation was used to avoid a rolling refresh effect.

Compared to previous work,[40] the quality of the chronoamperometric signal (Figure 6 a) has been greatly improved, both in terms of signal-to-noise ratio, and reduction in variation between the different working electrodes. This is due to the use of microelectrode arrays, which increase the signal without sacrificing the enhanced sensing properties of microelectrodes, and the reduction of parasitic capacitance, inductance and resistance in the device (Section 3.1).

Conformal fluid contact at the electrode sites is essential for this sensing protocol. In our experiment it was possible to ensure fluid contact by preparing the model eye prior to measurement (Section 2), and to manually check the data after measurement to confirm that there was no loss of the characteristic chronoamperometric sub-signal. However, it is worth noting that in a clinical setting loss of fluid contact is a likely to occur occasionally, and data processing algorithms should be designed with this contingency in mind, i.e. with the ability to detect loss of the chronoamperometric sub-signal and to discard or flag that particular measurement.

The result of this signal processing method is shown in (Figure 6 c), in which time-varying concentration data are shown for each working electrode during a beaker experiment. In this experiment, measurements were first performed in a beaker of KCl (0.1 M) and FeMeOH (0.5 mM) to produce calibration data as described above. Next, two 1 ml injections of FeMeOH (0.5 mM) were added to a beaker KCl (0.1 M, initial volume ~ 5 ml) during a 10 s measurement period. The effects of each injection are clearly visible in the plot, and the distribution of concentration across the device shows some spatial inhomogeneity resulting from the position of the ESCL in the beaker and the location of the pipette tip. At the moment of injection, the concentrations measured at each electrode are somewhat volatile (e.g. t = 7 to 8 s), reflecting agitation and bulk movement in the two miscible fluids. As time progresses subsequent to each injection, mixing effects begin to reduce the disparity in concentration between each working electrode (e.g. t = 9 to 10 s).

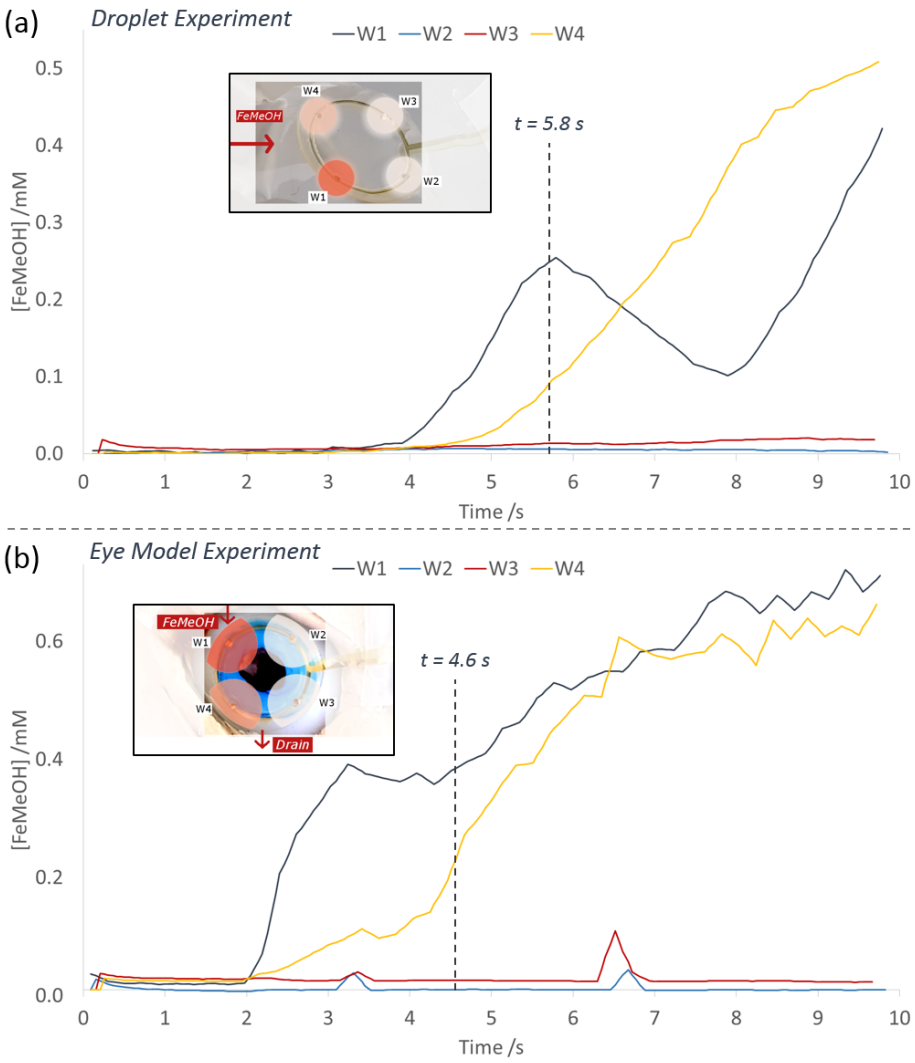

Figure 7. Concentration data for each working electrode during droplet and eye model experiments. (a) Concentration data for each working electrode during a 10 s droplet experiment, in which FeMeOH was pipetted into an initial droplet of KCl. Inset: visual representation of the concentration at each working electrode, with concentration values represented by red colour shading (see Video 2); (b) concentration data for each working electrode during a 10 s eye model experiment, in which FeMeOH was introduced to the fluid input of the eye model after previous irrigation with KCl. Inset: visual representation of the concentration at each working electrode, with concentration values represented by red colour shading (see Video 3).

To investigate the ESCL in environments more representative of the ocular surface, two more experiments were designed. Both experiments were performed multiple times, with representative results shown in **Figure 7**. In the first, the device was placed on top of a droplet of KCl for a zero

concentration calibration measurement, then FeMeOH for a high concentration calibration measurement, with electrodes facing down. After calibration, a time- and space-varying concentration was created by slowly injecting FeMeOH (~ 0.5 ml) into an initial droplet of KCl (~ 0.5 ml) at the W1 and W4 side of the ESCL (Figure 7 a). By injecting the FeMeOH slowly, bulk mixing was kept to a minimum, and very little increase in concentration was observed at W2 and W3, while W1 and W4 measured large changes in concentration. Flow of the droplet away from the ESCL towards the lower left direction during this experiment drew residual KCl into the W1 region, which resulted in a transient reduction in concentration from t = 6 to 8 s. As injection continued, both W1 and W4 measured an increasing concentration, with diffusive effects beginning to reach W3 by the end of the measurement period (t = 9 to 10 s).

In the second experiment, measurements were carried out on a model eye, built to mimic some aspects of the flow of tear film in the eye (Section 2). While blinking effects and viscosity play key roles in the flow of the lachrymal fluid in a real eye, this experiment was designed as a proof of principle, to show that (a) spatial variation in concentration can be measured in a flow environment at a high rate of change, and (b) the ESCL can work effectively on the curved surface of a structure similar to the eye. Since little is known about the flow of tear film in the eye when a contact lens is worn, there may be diminishing returns in creating more 'accurate' eye models; a more informative next step would be to work in an animal or human model.

FeMeOH was injected through the fluid input tube, located in a position analogous to the lachrymal ducts (Figure 7 b, see Figure 3 a). The flow of liquid was observed first at W1, then W4, at which point the fluid ran along the lower eyelid section of the model to the fluid output tube, located in a position analogous to the lachrymal puncta. Fluid was occasionally observed around the W3 region, although without blinking effects the transport of fluid to W2 and W3 was very limited. The eye model was irrigated with KCl before the input of FeMeOH; calibration from the droplet experiment was used to ensure a good fluid connection during those procedures.

The data measured from the four working electrodes shows evidence of all empirically observed fluid flow effects. W1 quickly measured a concentration change (t = 2 s), and after an initially steep increase, continued to increase more slowly as residual KCl was flushed out (t = 7 to 10 s). W4 measured an increase in FeMeOH concentration after an additional delay (t = 2.5 s), and, since the fluid was flowing over a larger area after the initial injection point when compared to W1, measured a slower increase in local concentration (t = 3 to 5 s). W2 and W3 measured a slight increase in concentration on occasion, when fluid happened to flow away from the ordinary path (e.g. t = 6.5 s). Slightly elevated concentrations were observed in the eye model experiment; this effect is due to fluid flow speed and diffusion region disruption, and is negligible in physiological flow conditions (see Appendix C for a more in-depth discussion).

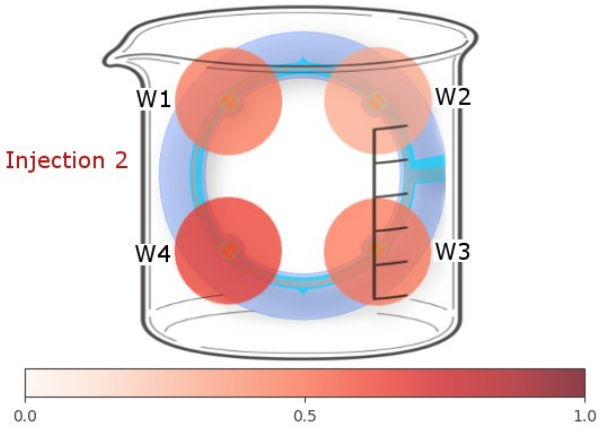

Video 1. Electrochemical video in which a colour map representation of FeMeOH concentration is used to visualise spatiotemporal concentration variation during the beaker experiment.

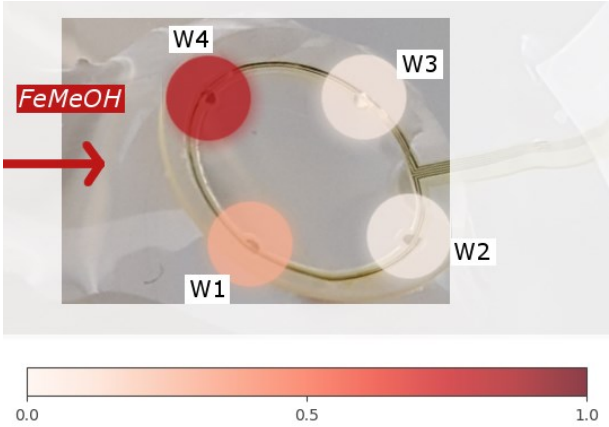

Video 2. Electrochemical video in which a colour map representation of FeMeOH concentration is used to visualise spatiotemporal concentration variation during the droplet experiment.

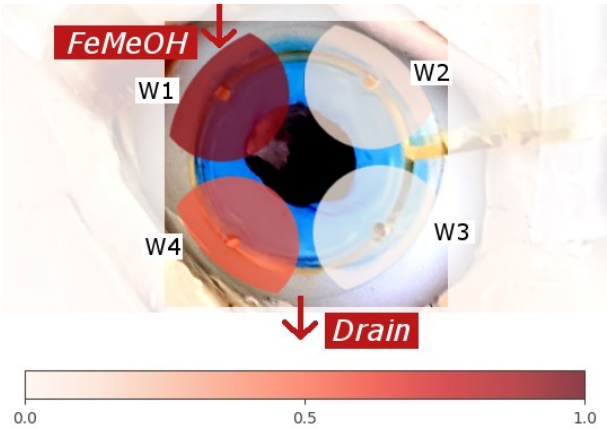

Video 3. Electrochemical video in which a colour map representation of FeMeOH concentration is used to visualise spatiotemporal concentration variation during the eye model experiment.

A spatiotemporal electrochemical measurement is intuitively visualised by an electrochemical 'video'. For each experiment, the data were rescaled between 0 and 1, and used to create a colour map, in which FeMeOH concentration was represented by the colour scale. These can be viewed in real time in **Videos 1-3**. These electrochemical 'videos' illustrate the various fluid effects discussed above.

4 Conclusions

We have demonstrated an ESCL with spatially distributed microelectrode arrays, capable of producing a real-speed electrochemical 'video' of spatiotemporal concentration variation across the surface of the cornea. This device represents a significant improvement on the utility of electrochemical measurements made in the eye, and progresses towards a new class of ESCL, able to produce sufficient data about biomarkers in the lachrymal fluid to help make useful diagnostic conclusions.

The design of the device builds on an existing SCL platform, which uses flexible biocompatible materials and standard cleanroom processes. Fabrication with polyimide and TPU achieved a

moulded SCL without any buckling, and the position of the gold traces in the neutral mechanical plane protected circuitry from damage during mechanical deformation. The platform offers a clear route to clinical use, and the design of the system is fully compatible with established integration technology such as chip integration and wireless power architecture.

The sensors performed well in electrochemical characterisation, with significant improvements on previous flexible microelectrodes in terms of sensitivity, power requirement and signal-to-noise ratio.[40] In spatiotemporal experiments, an updated version of the fast-switching chronoamperometric method produced video-rate electrochemical data from each electrode, in which a number of fluid effects could be observed. In an eye model, the device successfully tracked the flow of a high concentration fluid as it progressed across the ocular surface. Use of a single potentiostat with an analogue multiplexer allows for multiple electrodes to be integrated into one device without significantly increasing the footprint of the system.

In future, this device may be used to investigate real examples of tear flow across the cornea in an animal or human model. Integration of processing functionality could produce real-time electrochemical videos of the lachrymal fluid, and functionalisation of the microelectrode arrays may be carried out to select for various different biomarkers, such as glucose, lactate, cortisol or more. Future designs could also integrate additional electrode sites in each quadrant of the lens, functionalised differently to perform a suite of chemical measurements in the tear film. Using a wireless device operating continuously, and measuring multiple chemical markers concurrently, a new class of continuous, unobtrusive sensing system is within sight.

5 Acknowledgements

This work was supported by the EPSRC CDT in Integrative Sensing and Measurement, Grant Number EP/L016753/1 in the form of a studentship and additional travel allowance to support the collaborative activity with Ghent University. The authors would also like to thank Eva Gonzalez-Fernandez and Ilka Schmueser for their help in this work.

6 References

[1] Sensimed, (2015). http://www.sensimed.ch/en/.

[2] J. De Smet, A. Avci, P. Joshi, D. Schaubroeck, D. Cuypers, H. De Smet, Progress toward a liquid crystal contact lens display, J. Soc. Inf. Disp. 21 (2013) 399–406. doi:10.1002/jsid.188.

[3] C. Vanhaverbeke, R. Verplancke, J. De Smet, D. Cuypers, H. De Smet, Microfabrication of a spherically curved liquid crystal display enabling the integration in a smart contact lens, Displays. 49 (2017) 16–25. doi:10.1016/j.displa.2017.05.005.

[4] P. Mehta, L. Justo, S. Walsh, M.S. Arshad, C.G. Wilson, C.K. O'Sullivan, S.M. Moghimi, I.S. Vizirianakis, K. Avgoustakis, D.G. Fatouros, Z. Ahmad, New platforms for multi-functional ocular lenses: engineering double-sided functionalized nano-coatings, J. Drug Target. 23 (2015) 305–310. doi:10.3109/1061186X.2014.1001395.

[5] J. Pandey, Y.-T. Liao, A. Lingley, R. Mirjalili, B. Parviz, B.P. Otis, A Fully Integrated RF-Powered Contact Lens With a Single Element Display, IEEE Trans. Biomed. Circuits Syst. 4 (2010) 454–461. doi:10.1109/TBCAS.2010.2081989.

[6] J. Park, J. Kim, S.-Y. Kim, W.H. Cheong, J. Jang, Y.-G. Park, K. Na, Y.-T. Kim, J.H. Heo, C.Y. Lee, J.H. Lee, F. Bien, J.-U. Park, Soft, smart contact lenses with integrations of wireless circuits, glucose sensors, and displays, Sci. Adv. 4 (2018) eaap9841. doi:10.1126/sciadv.aap9841.

[7] H. Yao, Y. Liao, A.R. Lingley, A. Afanasiev, I. Lähdesmäki, B.P. Otis, B.A. Parviz, A contact lens with integrated telecommunication circuit and sensors for wireless and continuous tear glucose monitoring, J. Micromechanics Microengineering. 22 (2012) 075007. doi:10.1088/0960-1317/22/7/075007.

[8] N. Thomas, I. Lähdesmäki, B.A. Parviz, A contact lens with an integrated lactate sensor,

Sensors Actuators, B Chem. 162 (2012) 128–134. doi:10.1016/j.snb.2011.12.049.

[9] N.M. Farandos, A.K. Yetisen, M.J. Monteiro, C.R. Lowe, S.H. Yun, Contact lens sensors in ocular diagnostics, Adv. Healthc. Mater. 4 (2015) 792–810. doi:10.1002/adhm.201400504.

[10] A.J. Bandodkar, J. Wang, Non-invasive wearable electrochemical sensors: a review, Trends Biotechnol. 32 (2014) 363–371. doi:10.1016/j.tibtech.2014.04.005.

[11] S. Hagan, E. Martin, A. Enríquez-de-Salamanca, Tear fluid biomarkers in ocular and systemic disease: potential use for predictive, preventive and personalised medicine, EPMA J. 7 (2016) 15. doi:10.1186/s13167-016-0065-3.

[12] J.T. Baca, D.N. Finegold, S.A. Asher, Tear Glucose Analysis for the Noninvasive Detection and Monitoring of Diabetes Mellitus, Ocul. Surf. 5 (2007) 280–293. doi:10.1016/S1542-0124(12)70094-0.

[13] N.J. Van Haeringen, Clinical biochemistry of tears, Surv. Ophthalmol. 26 (1981) 84–96. doi:10.1016/0039-6257(81)90145-4.

[14] L.K. Banbury, Stress biomarkers in the tear film, Southern Cross University, 2009.

[15] B.S. McEwen, Protective and Damaging Effects of Stress Mediators, N. Engl. J. Med. 338 (1998) 171–179. doi:10.1056/NEJM199801153380307.

[16] F. Holsboer, The Corticosteroid Receptor Hypothesis of Depression, Neuropsychopharmacology. 23 (2000) 477–501. doi:10.1016/S0893-133X(00)00159-7.

[17] Y.I. Sheline, P.W. Wang, M.H. Gado, J.G. Csernansky, M.W. Vannier, Hippocampal atrophy in recurrent major depression, Proc. Natl. Acad. Sci. 93 (1996) 3908–3913. doi:10.1073/pnas.93.9.3908.

[18] R.S. Stawski, K.E. Cichy, J.R. Piazza, D.M. Almeida, Associations among daily stressors and salivary cortisol: Findings from the National Study of Daily Experiences,

Psychoneuroendocrinology. 38 (2013) 2654–2665. doi:10.1016/j.psyneuen.2013.06.023.

[19] W.R. Lovallo, Cortisol secretion patterns in addiction and addiction risk, Int. J. Psychophysiol. 59 (2006) 195–202. doi:10.1016/j.ijpsycho.2005.10.007.

[20] D.L. Delahanty, A.J. Raimonde, E. Spoonster, Initial posttraumatic urinary cortisol levels predict subsequent PTSD symptoms in motor vehicle accident victims, Biol. Psychiatry. 48 (2000) 940–7. http://www.ncbi.nlm.nih.gov/pubmed/11074232 (accessed June 3, 2019).

[21] J. De Smet, A. Avci, R. Beernaert, D. Cuypers, H. De Smet, Design and wrinkling behavior of a contact lens with an integrated liquid crystal light modulator, IEEE/OSA J. Disp. Technol. 8 (2012) 299–305. doi:10.1109/JDT.2012.2183575.

[22] A. Vásquez Quintero, R. Verplancke, H. De Smet, J. Vanfleteren, Stretchable Electronic Platform for Soft and Smart Contact Lens Applications, Adv. Mater. Technol. 2 (2017) 1700073. doi:10.1002/admt.201700073.

[23] R.R. Richardson, J.A. Miller, W.M. Reichert, Polyimides as biomaterials: preliminary biocompatibility testing, Biomaterials. 14 (1993) 627–635. doi:10.1016/0142-9612(93)90183-3.

[24] P. Starr, C.M. Agrawal, S. Bailey, Biocompatibility of common polyimides with human endothelial cells for a cardiovascular microsensor, J. Biomed. Mater. Res. Part A. 104 (2016) 406–412. doi:10.1002/jbm.a.35578.

[25] HD MicroSystems, PI-2600 Series – Low Stress Applications, (2009) 1–4. https://www.dupont.com/content/dam/dupont/products-and-services/electronic-and-electrical-materials/semiconductor-fabrication-and-packaging-materials/documents/PI-2600_ProcessGuide.pdf.

[26] A. Georgiev, D. Dimov, E. Spassova, J. Assa, P. Dineff, G. Danev, Chemical and Physical Properties of Polyimides: Biomedical and Engineering Applications, in: High Perform.

Polym. - Polyimides Based - From Chem. to Appl., InTech, 2012. doi:10.5772/53918.

[27] S.R.I. Gabran, M.T. Salam, J. Dian, Y. El-Hayek, J.L. Perez Velazquez, R. Genov, P.L. Carlen, M.M.A. Salama, R.R. Mansour, 3-D Flexible Nano-Textured High-Density Microelectrode Arrays for High-Performance Neuro-Monitoring and Neuro-Stimulation, IEEE Trans. Neural Syst. Rehabil. Eng. 22 (2014) 1072–1082. doi:10.1109/TNSRE.2014.2322077.

[28] F. Waschkowski, S. Hesse, A. Rieck, T. Lohmann, C. Brockmann, T. Laube, N. Bornfeld, G. Thumann, P. Walter, W. Mokwa, S. Johnen, G. Roessler, Development of very large electrode arrays for epiretinal stimulation (VLARS), Biomed. Eng. Online. 13 (2014) 11. doi:10.1186/1475-925X-13-11.

[29] T. Li, B. Sun, K. Xia, Q. Zeng, T. Wu, M.S. Humayun, Design and fabrication of a high-density flexible microelectrode array, in: 2017 IEEE 12th Int. Conf. Nano/Micro Eng. Mol. Syst., IEEE, 2017: pp. 299–302. doi:10.1109/NEMS.2017.8017029.

[30] M. Donora, I. Underwood, 70-4: Late-News Paper: Electronic Contact Lens for Senses beyond Sight, SID Symp. Dig. Tech. Pap. 50 (2019) 996–999. doi:10.1002/sdtp.13094.

[31] P. Alves, R. Cardoso, T.R. Correia, B.P. Antunes, I.J. Correia, P. Ferreira, Surface modification of polyurethane films by plasma and ultraviolet light to improve haemocompatibility for artificial heart valves, Colloids Surfaces B Biointerfaces. 113 (2014) 25–32. doi:10.1016/j.colsurfb.2013.08.039.

[32] J. Kim, M. Kim, M.S. Lee, K. Kim, S. Ji, Y.T. Kim, J. Park, K. Na, K.H. Bae, H.K. Kim, F. Bien, C.Y. Lee, J.U. Park, Wearable smart sensor systems integrated on soft contact lenses for wireless ocular diagnostics, Nat. Commun. 8 (2017). doi:10.1038/ncomms14997.

[33] K. Kim, Y. Park, B.G. Hyun, M. Choi, J. Park, Recent Advances in Transparent Electronics with Stretchable Forms, Adv. Mater. 31 (2019) 1804690. doi:10.1002/adma.201804690.

[34] J.T. Baca, C.R. Taormina, E. Feingold, D.N. Finegold, J.J. Grabowski, S.A. Asher, Mass Spectral Determination of Fasting Tear Glucose Concentrations in Nondiabetic Volunteers, Clin. Chem. 53 (2007) 1370–1372. doi:10.1373/clinchem.2006.078543.

[35] B. Peng, J. Lu, A.S. Balijepalli, T.C. Major, B.E. Cohan, M.E. Meyerhoff, Evaluation of enzyme-based tear glucose electrochemical sensors over a wide range of blood glucose concentrations, Biosens. Bioelectron. 49 (2013) 204–209. doi:10.1016/j.bios.2013.05.014.

[36] U. Stahl, M. Willcox, F. Stapleton, Osmolality and tear film dynamics, Clin. Exp. Optom. 95 (2012) 3–11. doi:10.1111/j.1444-0938.2011.00634.x.

[37] A. Tomlinson, S. Khanal, Assessment of Tear Film Dynamics: Quantification Approach, Ocul. Surf. 3 (2005) 81–95. doi:10.1016/S1542-0124(12)70157-X.

[38] I. Schmueser, A.J. Walton, J.G. Terry, H.L. Woodvine, N.J. Freeman, A.R. Mount, A systematic study of the influence of nanoelectrode dimensions on electrode performance and the implications for electroanalysis and sensing, Faraday Discuss. 164 (2013) 295. doi:10.1039/c3fd00038a.

[39] R.M. Wightman, Voltammetry with Microscopic Electrodes in New Domains, Science (80-.). 240 (1988) 415–420. doi:10.1126/science.240.4851.415.

[40] M. Donora, E. Gonzalez-Fernandez, A. Vásquez Quintero, H. De Smet, I. Underwood, Spatiotemporal electrochemistry on flexible microelectrode arrays: Progress towards smart contact lens integration, Sensors Actuators B Chem. 296 (2019) 126671. doi:10.1016/j.snb.2019.126671.

[41] Arduino Nano Guide, (n.d.). https://www.arduino.cc/en/Guide/ArduinoNano.

[42] R. Verplancke, F. Bossuyt, D. Cuypers, J. Vanfleteren, Thin-film stretchable electronics technology based on meandering interconnections: Fabrication and mechanical performance, J. Micromechanics Microengineering. 22 (2012). doi:10.1088/0960-1317/22/1/015002.

[43] M.D. Young, W.J. Benjamin, Oxygen Permeability of the Hypertransmissible Contact Lenses, Eye Contact Lens Sci. Clin. Pract. 29 (2003) S17–S21. doi:10.1097/00140068-200301001-00006.

[44] I. Schmüser, The design, fabrication and characterisation of nanoelectrodes for electrochemical sensing, (2015).

[45] M. Gordic, Theoretical modeling of cortisol sensor, (2008) 71. http://scholarcommons.usf.edu/etdhttp://scholarcommons.usf.edu/etd/267 (accessed May 23, 2019).

[46] Y.-T. Liao, H. Yao, A. Lingley, B. Parviz, B.P. Otis, A 3-uW CMOS Glucose Sensor for Wireless Contact-Lens Tear Glucose Monitoring, IEEE J. Solid-State Circuits. 47 (2012) 335–344. doi:10.1109/JSSC.2011.2170633.

[47] K. Mansouri, T. Shaarawy, Continuous intraocular pressure monitoring with a wireless ocular telemetry sensor: initial clinical experience in patients with open angle glaucoma, Br. J. Ophthalmol. 95 (2011) 627–629. doi:10.1136/bjo.2010.192922.

[48] M. Nasreldin, R. Delattre, M. Ramuz, C. Lahuec, T. Djenizian, J.-L. de Bougrenet de la Tocnaye, Flexible Micro-Battery for Powering Smart Contact Lens, Sensors. 19 (2019) 2062. doi:10.3390/s19092062.

[49] J.I. Prydal, P. Artal, H. Woon, F.W. Campbell, Study of human precorneal tear film thickness and structure using laser interferometry., Invest. Ophthalmol. Vis. Sci. 33 (1992) 2006–11. http://www.ncbi.nlm.nih.gov/pubmed/1582805 (accessed June 3, 2019).

[50] U.A. Aregueta-Robles, A.J. Woolley, L.A. Poole-Warren, N.H. Lovell, R.A. Green, Organic electrode coatings for next-generation neural interfaces, Front. Neuroeng. 7 (2014). doi:10.3389/fneng.2014.00015.

[51] Q. Yu, J.M. Bauer, J.S. Moore, D.J. Beebe, Responsive biomimetic hydrogel valve for

microfluidics, Appl. Phys. Lett. 78 (2001) 2589–2591. doi:10.1063/1.1367010.

[52] H. Yao, A.J. Shum, M. Cowan, I. Lähdesmäki, B.A. Parviz, A contact lens with embedded sensor for monitoring tear glucose level, Biosens. Bioelectron. 26 (2011) 3290–3296. doi:10.1016/j.bios.2010.12.042.

[53] Y. Saito, A Theoretical Study on the Diffusion Current at the Stationary Electrodes of Circular and Narrow Band Types, Rev. Polarogr. 15 (1968) 177–187. doi:10.5189/revpolarography.15.177.

[54] P.N. Bartlett, S.L. Taylor, An accurate microdisc simulation model for recessed microdisc electrodes, J. Electroanal. Chem. 453 (1998) 49–60. doi:10.1016/S0022-0728(98)00242-3.

[55] A.D. McNaught, A. Wilkinson, IUPAC, Compendium of Chemical Terminology, 2nd Editio, Blackwell Scientific Publications, 1997.